

# Study on the giant magnetoimpedance effect in micro-patterned Co-based amorphous ribbons with single strip structure and tortuous shape

Zhen Yang · Chong Lei · Yong Zhou · Xue-cheng Sun

Received: 5 July 2014 / Accepted: 1 October 2014 / Published online: 21 October 2014  
© Springer-Verlag Berlin Heidelberg 2014

**Abstract** Field-annealed Co-based commercial amorphous ribbons (Metglas<sup>®</sup> 2714A) with single strip structure and tortuous shape are fabricated by MEMS technology. The influence of the size, magnetic field and frequency on the giant magnetoimpedance (GMI) ratio of the ribbons with single strip structure and tortuous shape is investigated. The results show that the GMI ratio of micro-patterned Co-based amorphous ribbons with single strip structure increases with increasing in length and decreases with the increasing in width. The ribbons (length = 10 mm, width = 250  $\mu\text{m}$ ) with single strip can get higher GMI ratio at lower frequency (<40 MHz). The GMI ratio of micro-patterned tortuous-shaped Co-based amorphous ribbon with six turns is biggest with 82 %, obtained at a frequency of 40 MHz and a field of 20 Oe, and the GMI ratio increases with the increasing in turn number from two turns to six turns. All mechanisms (line width and tortuous shape) that influence the inductance and resistance will result in changes in the impedance and the GMI effect. The anisotropy field  $H_K$  (15–20 Oe) of tortuous shape ribbon that the peak GMI ratio is larger than that (5–10 Oe) of the ribbon with single strip structure. The effect of the frequency on the GMI ratio of the ribbons with tortuous shape is more complex. This can be explanation by complex inductance of tortuous shape ribbons.

## 1 Introduction

The giant magnetoimpedance (GMI) effect is a change in the complex impedance at high frequency (usually >0.1 MHz) and arises from the magnetic field-induced change of the dynamic relative permeability  $\mu_r$  of the magnetic material. The GMI-based magnetic sensors have several advantages (smaller size, high sensitivity, higher stability and lower power), so the GMI effect is extensively studied in soft amorphous ferromagnetic wires (Atalay et al. 2006; Li et al. 2003), thin film (Zhou et al. 2001; Makhnovskiy et al. 2004), and ribbons (Yang et al. 2014; Chen et al. 2009a, b) in order to produce high-performance and practical GMI-based sensors. In today's word, the GMI-based magnetic sensors are widely used in electronic compass, magnetic ink reading, vehicle detection, non-destructive testing of metals, detection of biomarkers, and so on.

The GMI effect of the amorphous ribbon may be related to the high transverse permeability caused by the transversely oriented domain configuration (Panina et al. 1995). The amorphous ribbon has low magnetostriction and controlled magnetic anisotropy, so much work has been done on the GMI effect in soft magnetic Co-based amorphous wires and ribbons (Beach and Berkowitz 1994; Sommer and Chine 1996; Jang et al. 2000). Recent years, some biosensor prototypes based on GMI effect of the amorphous ribbon with single strip structure (Kurlyandskaya et al. 2003; Devkota et al. 2013; Yang et al. 2010) and tortuous shape (Chen et al. 2011; Yang et al. 2010) were introduced into biosensing field. So, it is very significant to observe the effect of size, magnetic field and frequency on the GMI ratio of the ribbons with single strip structure and tortuous shape. Chaturvedi et al. (2010) reported a systematic study of the influence of sample

---

Z. Yang · C. Lei · Y. Zhou (✉) · X. Sun  
Key Laboratory for Thin Film and Microfabrication of the  
Ministry of Education, Department of Micro/Nano Electronics,  
School of Electronic Information and Electrical Engineering,  
Shanghai Jiao Tong University, Dong Chuan Road 800,  
Shanghai 200240, People's Republic of China  
e-mail: yzhou@sjtu.edu.cn

Z. Yang  
e-mail: zhc025@sjtu.edu.cn

length on the GMI effect and its field sensitivity ( $\%/Oe$ ) in  $Co_{69}Fe_{4.5}Ni_{1.5}Si_{10}B_{15}$  amorphous ribbons with single stripe and a width of 1 mm in the frequency range of 0.1–10 MHz. The influence of varying width from 4 mm down to 300  $\mu m$  on the GMI effect in soft ferromagnetic amorphous  $Co_{65}Fe_4Ni_2Si_{15}B_{14}$  ribbons with single stripe and a length of 1 cm was investigated by Devkota et al. (2014). The effect of length and width on the GMI effect in micro-patterned Co-based ribbons with a meander structure was investigated by Yang et al. (2014). Chen et al. (2009a, b) revealed that the maximum GMI ratio was got in the three-turns meander ribbon with 600  $\mu m$  line width at a frequency of 20 MHz and a field of 10 Oe, however, the designed length of 10 mm was a little bit of large. In order to meet the requirements of biosensor using amorphous ribbon to detect the biomarker, a miniaturization technology of amorphous ribbon is needed, and MEMS technology is the best choice for the micro-sized GMI-based sensor. It is possible to use amorphous ribbons in more biosensing fields.

So, in this context, micro-patterned Co-based amorphous ribbons (Metglas<sup>®</sup> 2714A) with single strip structure and tortuous shape were fabricated by MEMS technology. The GMI ratio of the with single strip structure (length = 5 mm, width = 250  $\mu m$ ) and tortuous shape (length = 5 mm, width = 250  $\mu m$ , and turn number = 6) at different magnetic fields (0–60 Oe) and frequencies (1–40 MHz) was discussed. The influence of different length (5 and 10 mm) and widths (250–2000  $\mu m$ ) on the GMI ratio of the ribbons with single strip structure was observed, and at the same width and length, the GMI ratio of the ribbon with single strip structure was compared with those in the ribbons with tortuous shape of varying turn numbers from two turns to six turns.

## 2 Experimental procedures

In this section, the micro-patterned GMI sensor elements were made of a Co-based commercial amorphous ribbon (Metglas<sup>®</sup> 2714A). The main physical and magnetic properties of the ribbons were listed in Table 1.

Before MEMS processing, some rectangular ribbons (20  $\mu m$  thick, 5 cm wide and 8 cm long) were annealed with an applied magnetic field along the transverse direction of the sample to induce a transverse anisotropy. A transverse induced anisotropy was evident from the magnetization curve as shown in Fig. 1. The whole annealing processing was finished in a small vacuum chamber within which the ribbon was fixed firmly. A permanent magnet was placed at the center of chamber with 200 Oe field strength. It took 1.5 h to reach the annealing temperature of 250 °C (higher than the Curie point of Co-based ribbon).

**Table 1** The main physical and magnetic properties of commercial ribbon

Parameters	2714A
Saturation induction $B_S$ (T)	0.57
Saturation magnetostriction	$<1 \times 10^{-6}$
Maximum permeability $\mu_{max}$	$5 \times 10^5$
Curie temperature (°C)	225
Coercivity $H_c$ (A/m)	2

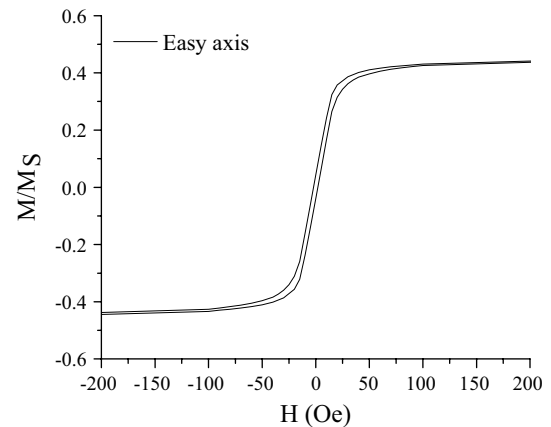
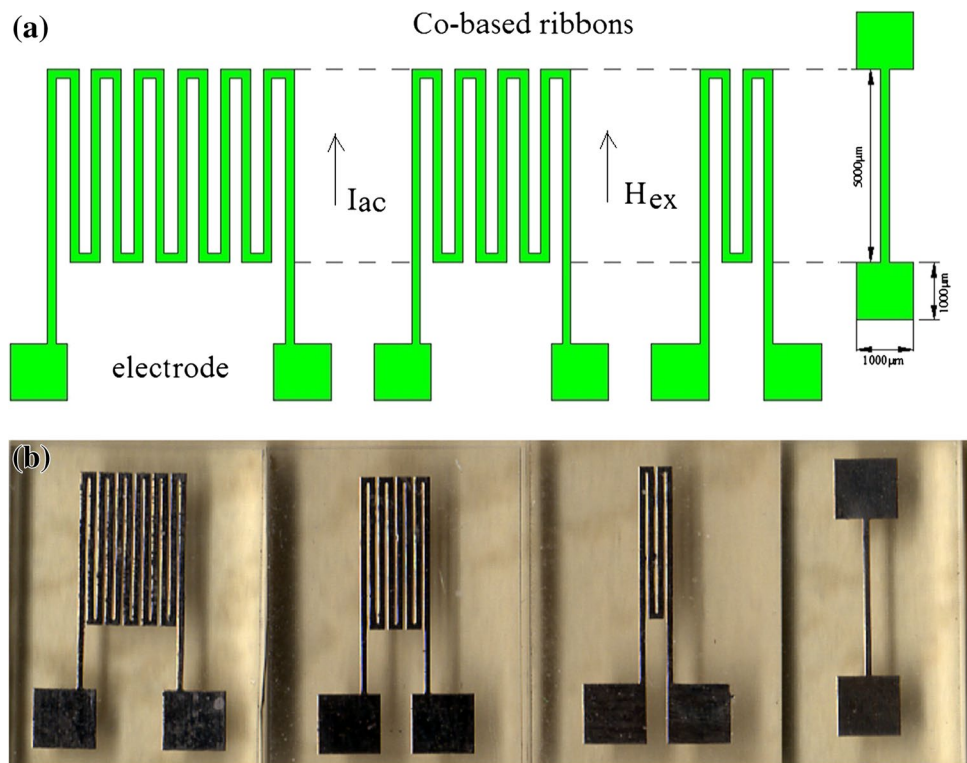


**Fig. 1** Transverse hysteresis loop of the field-annealed ribbon

When the temperature reached to 250 °C, heating was kept on this temperature for 3 h and then it took 5 h to cool down to room temperature gradually.

The micro-patterned ribbons with single strip structures and tortuous shape (two-turn, four-turn, and six-turn structures) (as shown in Fig. 2a) were designed with width of 250  $\mu m$  and length of 5 mm. In addition, the micro-patterned ribbons with single strip structures were designed with different widths (250, 500, 1,000, 1,500, 2,000  $\mu m$ ) and length of 10 mm. The intervals of tortuous shape were 30  $\mu m$ . Each 'n' shape in the meander structures was called one turn. The ribbons with different structures were fabricated by photolithography and chemical etching methods. Firstly, the ribbon was bound on clean glass substrates using an epoxy adhesive, during binding we should try to ensure tight bonding and no air between the ribbon and the substrate. And then photoresist coating with thickness of 10  $\mu m$  was spun on the surface of the ribbon and patterned by lithography. At last, the ribbon was etched in an acidic mixed solution (mixture of  $HNO_3$ ,  $HCl$ ,  $H_2O_2$  and  $H_2O$  with a certain proportion) for 5 min. After removing photoresist layer, we got the micro-patterned Co-based ribbons with different structures as shown in Fig. 2b. The micro-patterned ribbons with single strip structures and the length of 10 mm were not shown here.

**Fig. 2** **a** Top view of the micro-patterned ribbon with different structure; **b** photograph of the samples after etching process



The GMI effects in micro-patterned ribbon were measured by an impedance analyzer (HP4194A) in the frequency range of 1–40 MHz with the constant current amplitude of 10 mA. An external magnetic field ( $H_{ex}$ ) of 1–60 Oe was applied along the longitudinal direction of the sample. Magnetic field is got from a permanent, the magnitude of that was controlled through changing the distance between the permanent and micro-patterned ribbon. The permanent slowly closed to the ribbon along the central axis of ribbon. Magnetic fields at different locations were measured strictly by a magnetometer, so the different marked locations stood for different magnetic fields (Yang et al. 2014). Figure 2a shows the different structures of patterned ribbons and the direction of the AC current and external magnetic field. The GMI ratio is defined as:  $GMI\ ratio\ (100\ \%) = 100\ \% \times [Z(H) - Z(H_0)]/Z(H_0)$ , where  $Z(H)$  and  $Z(H_0)$  are the magnetoimpedance with and without magnetic field, respectively.

### 3 Results and discussion

Figure 3 shows field and frequency dependence of the GMI ratio for micro-patterned Co-based amorphous ribbons with single strip structures ( $l = 5\ mm$ ,  $w = 250\ \mu m$ ). In sample testing, an external magnetic field of 1–60 Oe is applied along the longitudinal direction of the meander ribbon and is perpendicular to the transverse anisotropy direction of the sample.

The maximum GMI ratio is 44 % and obtained at  $H_{ex} = 10\ Oe$  and frequency  $f = 40\ MHz$ . On increasing the applied magnetic field  $H_{ex}$ , the magnitude of the GMI ratio first reaches a sharp peak and then gradually decreases to zero and even negative values. This typical characteristic has been observed by Sommer and Chine (1996). Sommer indicates that a longitudinal GMI spectrum of soft magnetic materials with high transverse permeability has the typical characteristic. The GMI curves in Fig. 3a agree well with this typical characteristic, which can be explained by the magnetization rotation model (Kumar et al. 2007; Amalou and Gijs 2001) and it goes as follows: the rotational magnetic permeability related to the GMI ratio increases with the increase in  $H_{ex}$  and reaches a maximum value as  $H_{ex} = H_K$ , where  $H_{ex}$  is perpendicular to the transverse anisotropy direction of the sample and  $H_K$  is the anisotropy field. Thereafter, the permeability decreases with  $H_{ex}$  and the GMI ratio gradually drops. The anisotropy field  $H_K$  of the ribbons with single strip structure is different at different frequency as can be seen in Fig. 3a. Besides, we can find the GMI curve at the frequency of 40 MHz is different from others. In the rage of 0–10 Oe, the GMI ratio changes drastically, and sometimes does not exceed to the value at low frequency.

It is observed that all the maximum values are obtained at 40 MHz (named as relaxation frequency), The relaxation frequency, where the peak GMI ratio is located, are the same under different magnetic fields and got in the measuring

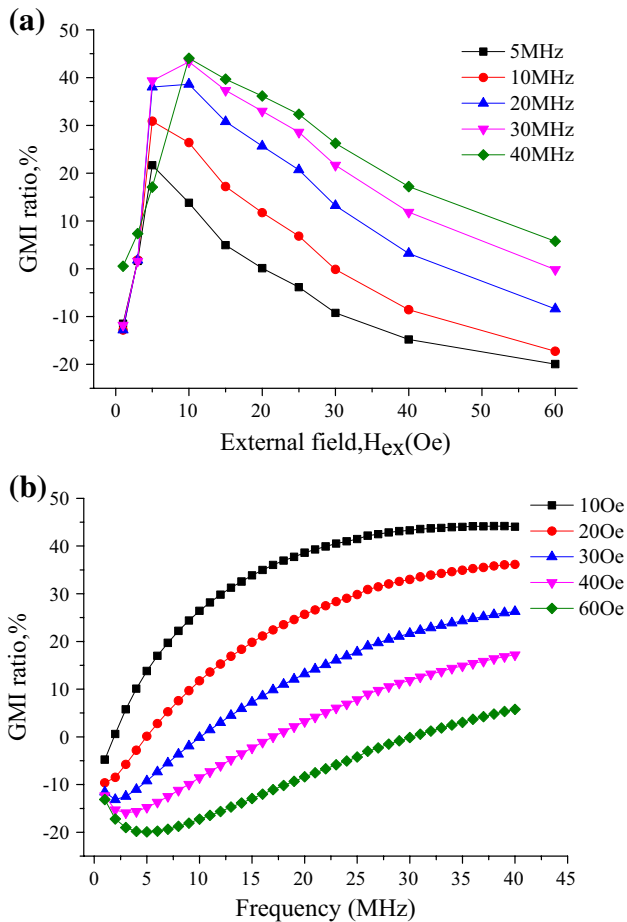


**Fig. 3** **a** Field and **b** frequency dependence of the GMI ratio of the ribbons with single strip structures ( $l = 5$  mm,  $w = 250$   $\mu\text{m}$ )

range of 1–40 MHz. However, it tends to move upward with the increase of measuring range of frequency, this is different from that mentioned in some work (Jang et al. 2000; Prida et al. 2003). The GMI ratios tend to move upward all the time when the magnetic field  $H_{ex} = 10$ –30 Oe, and the GMI ratio first decreases and then increases to the peak GMI ratio when the magnetic field  $H_{ex} = 40$ –60 Oe as can be seen in Fig. 3b. The curves have no intersection. The frequency dependence of the GMI ratio of the ribbon can be explained with two different magnetization mechanisms, called domain wall movement and magnetization rotation, which dominates in lower and higher frequency ranges, respectively. In the low frequency range (1 MHz to several MHz), the GMI effect originates mainly from the variation of the skin depth, due to a strong change in the effective permeability caused by the external field  $H_{ex}$  (Phan and Peng 2008), in the high frequency range (several tens of MHz), reduction in the GMI ratio is related to the fact that the domain walls become strongly damped by the eddy current and only magnetization rotation contributes to GMI.

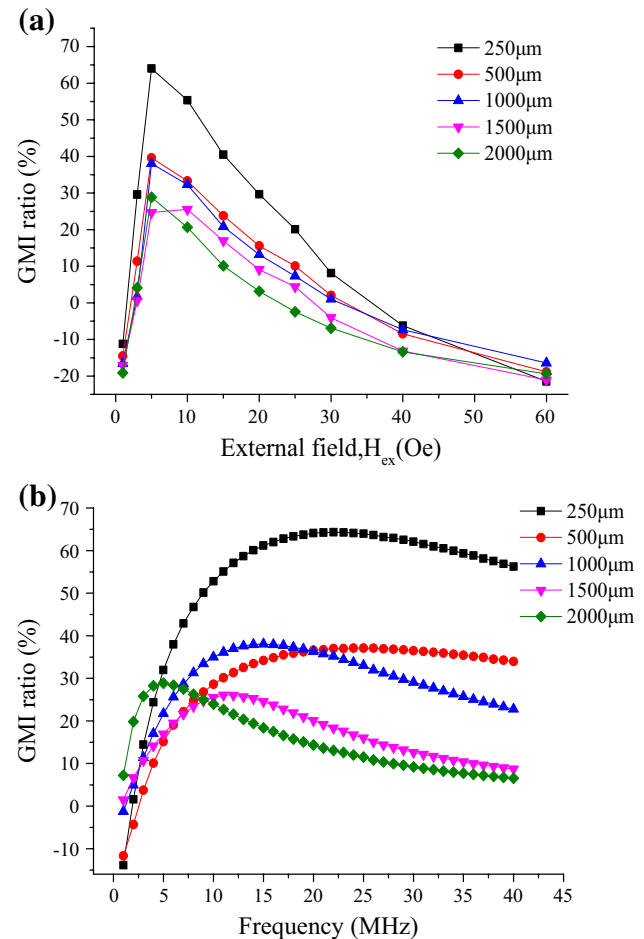


**Fig. 4** **a** Field and **b** frequency dependence of the GMI ratio of the single strip-structured ribbons with different widths ( $l = 10$  mm)

The micro-patterned ribbons with single strip structure were designed with different widths (250, 500, 1,000, 1,500, 2,000  $\mu\text{m}$ ) and length of 10 mm to observe the effect of size on GMI ratio (Fig. 4). It is obvious the maximum of GMI ratio (64 %) in the single strip-structured sample with 250  $\mu\text{m}$  width and 10 mm length is large than that mentioned above (43 %). From the previous work (Yang et al. 2014), the increase of the length from 5 mm to 10 mm led to an increase of the GMI effect. In present work, we only observed two lengths of 5 and 10 mm on the effect of GMI ratio, and we think the GMI ratio increases with the increasing of length from 5 to 10 mm. This is different from the report made by Chaturvedi et al. (2010), Chaturvedi considers that there exists a critical length ( $\sim 8$  mm) below which the maximum GMI decrease with decreasing sample length ( $L$ ) and above which they increase with decreasing  $L$ . Different raw material composition and thermal treatment may be used to explain it. The increase of the length of the sample may result in an increase in magnetized uniformity and soft magnetic properties. The length

of micro-patterned ribbons with single strip structures used in biosensing field was usually more than or equal to 10 mm (Kurlyandskaya et al. 2003; Devkota et al. 2013; Yang et al. 2010; Chen et al. 2011), so the sample with 10 mm length was designed. From the Fig. 4a, at the frequency of 40 MHz, we can find the maximum of the GMI ratio decrease from 64 % in the sample with 250 μm width to 24 % in the 2,000 μm sample. The  $H_K$  of the different-width ribbon with single strip structure is 5–10 Oe. The frequency dependence of the GMI ratio for single strip-structured ribbons with different widths is shown in Fig. 4b, and the GMI ratios of different line-width samples are chose at the  $H_K$ . We can find the maximum of the GMI ratio are obtained at the frequency <40 MHz (22 MHz for 250 μm, 24 MHz for 500 μm, 15 MHz for 1,000 μm, 11 MHz for 1,500 μm and 5 MHz for 2,000 μm). The high frequency is not advisable in practical application. The experimental results show the ribbons (length ≥10 mm) with single strip may be used in biosensing field (Kurlyandskaya et al. 2003; Devkota et al. 2013; Yang et al. 2010; Chen et al. 2011). Compared with the research (Chaturvedi et al. 2010; Devkota et al. 2014), smaller size (width = 250 μm) and wider operational frequency of the ribbon are observed.

The field and frequency dependence of the GMI ratio of the tortuous-shaped ribbons with six turns ( $l = 5$  mm,  $w = 250$  μm) are shown in Fig. 5. The maximum GMI ratios of six turns structure is 82 %. The relaxation frequency is 40 MHz. According to the definition of  $H_K$  mentioned above, the  $H_K$  of the ribbon of tortuous shaped is 15–20 Oe. The field dependence of the GMI ratio of the tortuous-shaped ribbons (Fig. 5a) has the same variation trend compared with Fig. 3a, so the same explanation of the mechanism can be presented mentioned above. In Fig. 5a, the anisotropy field  $H_K$  of patterned ribbons that the peak GMI ratio varies in the range of 15–20 Oe (15 Oe for 5–10 MHz and 20 Oe for 20–40 MHz).

On increasing the frequency, the GMI ratio of the ribbon with six turns urges intersection at different magnetic field (Fig. 5b), we consider the complex magnetic interaction between turns is the main result. With respect to impedance when an ac current with a high frequency is applied to a ferromagnetic material and the skin effect appears, the impedance  $Z$  can be expressed as follows:  $Z = R(\omega, \mu) - j X(\omega, \mu) = R(\omega, \mu) - j \omega [L_s(\omega, \mu) + L_m(\omega, \mu)]$ , where  $R$  is the resistance,  $X$  is the reactance,  $L_s$  is the self-inductance,  $L_m$  is the mutual inductance, inductance  $L = L_s + L_m$ ,  $\omega$  is the ac current frequency and  $\mu$  is the permeability of the conductor, which changes with  $H_{ex}$  and  $\omega$ . For the tortuous-shaped ribbon,  $L_m$  is very complex and the main reason leading to the great change of the GMI effect, because several factors should be considered, such as distribution of the magnetic field in the conductor and exterior space, distribution of the ac current, magnetic interaction among

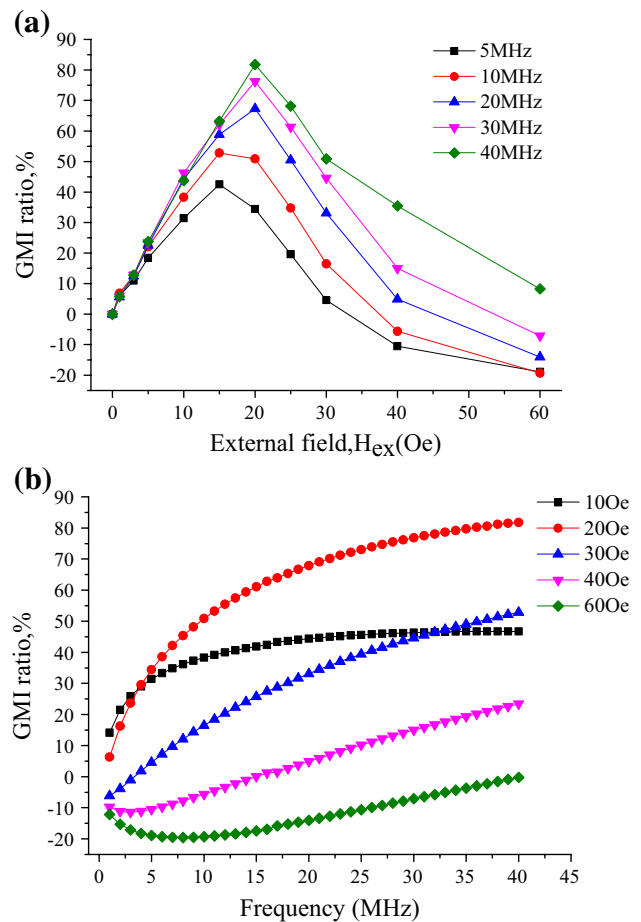


**Fig. 5** a Field and b frequency dependence of the GMI ratio of the tortuous-shaped ribbons with six turns ( $l = 5$  mm,  $w = 250$  μm)

each individual line segment, effect of the domain structure, and the magnetoelastic anisotropies on permeability and so on.

Figure 6 shows field and frequency dependence of the GMI ratio of the tortuous-shaped ribbons with different turns ( $l = 5$  mm,  $w = 250$  μm). And the GMI ratios of different samples in Fig. 6b are chose at the  $H_K$  and different frequencies. The results show that the GMI ratios of the ribbons with tortuous shape are larger than that of the ribbon with single strip-structured ribbon. This result is identical with the previous research by Chen et al. (2009a, b). Compared with the research, we design small length and investigate the influence of more turns number on GMI ratio of the ribbon with tortuous shape. The maximum of the GMI ratio increases from 44 % for the single strip-structured sample to the 82 % for the sample with six turns. This can be explained from the point of view of inductance. When the ac current flows through the tortuous ribbon, just as for the flux in each longitudinal and transverse straight line in a plane inductance, the fluxes will correlate with each other by mutual inductance of the magnetic chains. This is higher

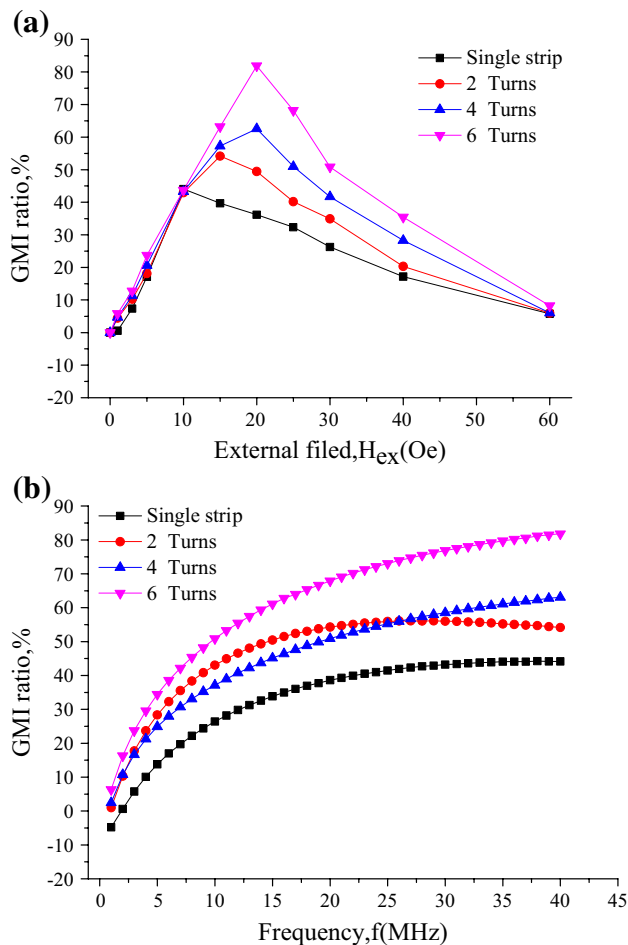


**Fig. 6** **a** Field and **b** frequency dependence of the GMI ratio of the tortuous-shaped ribbons with different turns ( $l = 5$  mm,  $w = 250$   $\mu$ m)

than the self-inductance of a single strip structure and the more turns of the meander structure, the more intense the interaction becomes. As a result, these effects lead to the increase in  $L_m$  and  $Z$ . Although the maximum of the GMI ratio (82 %) is largest, the work frequency was a little high. So Co-based amorphous ribbon with tortuous shape should be further studied in biosensing field, the aim is to get high GMI ratio at lower frequency and smaller size.

#### 4 Conclusion

In conclusion, the GMI ratio of micro-patterned Co-based amorphous ribbon with single strip structure increases with increasing in length and decreases with the increasing in width. The increase of the length of the sample may result in an increase in magnetized uniformity and soft magnetic properties. The ribbon (length = 10 mm) with single strip structure can get higher GMI ratio at lower frequency (<40 MHz). The GMI ratio of micro-patterned

tortuous-shaped Co-based amorphous ribbon with six turns is biggest with 82 %, obtained at a frequency of 40 MHz and a field of 20 Oe, and the GMI ratio increases with the increasing of turn from two turn to six turns. All mechanisms (line width and tortuous shape) that influence the inductance and resistance will result in changes in the impedance and the GMI effect. The anisotropy field  $H_K$  (15–20 Oe) of tortuous-shaped ribbon that the peak GMI ratio is larger than that (5–10 Oe) of the ribbon with single strip structure. The effect of the frequency on the GMI ratio of the ribbons with tortuous shape is more complex. This can be explanation by complex inductance of tortuous shape ribbon.

**Acknowledgments** This work was supported by The National Natural Science Foundation of China (No. 61074168 and No. 61273065), National Science and Technology Support Program (2012BAK08B05), National Key Laboratory Research Fund (9140C790403110C7905), Natural Science Foundation of Shanghai (13ZR1420800) and the Analytical and Testing Center in Shanghai Jiao Tong University.

#### References

- Amalou F, Gijjs MAM (2001) Giant magnetoimpedance of chemically thinned and polished magnetic amorphous ribbons. *J Appl Phys* 90:3466. doi:10.1063/1.1398072
- Atalay FE, Kaya H, Atalay S (2006) Magnetoimpedance effect in electroplated NiFeRu/Cu wire. *J Phys D* 39:431. doi:10.1088/0022-3727/39/3/001
- Beach RS, Berkowitz A (1994) Giant magnetic field dependent impedance of amorphous FeCoSiB wire. *Appl Phys Lett* 64:3652–3654. doi:10.1063/1.111170
- Chaturvedi A, Dhakal TP, Witanachchi S, Le AT, Phan MH, Srikantha H (2010) Critical length and giant magnetoimpedance in  $\text{Co}_{69}\text{Fe}_4\text{Ni}_{1.5}\text{Si}_{10}\text{B}_{15}$  amorphous ribbons. *Mater Sci Eng, B* 172:146–150. doi:10.1016/j.mseb.2010.04.038
- Chen L, Zhou Y, Zhou ZM, Ding W (2009a) Effect of meander structure and line width on GMI effect in micro-patterned Co-based ribbon. *J Phys D* 42:145005. doi:10.1088/0022-3727/42/14/145005
- Chen L, Zhou Y, Zhou ZM, Ding W (2009b) Enhancement of magnetoimpedance effect in Co-based amorphous ribbon with a meander structure. *Phys Status Solidi A* 206:1594. doi:10.1002/pssa.200925024
- Chen L, Bao CC, Yang H, Lei C, Zhou Y, Cui DX (2011) A prototype of giant magnetoimpedance-based biosensing system for targeted detection of gastric cancer cell. *Biosens Bioelectron* 26:3246–3253. doi:10.1016/j.bios.2010.12.034
- Devkota J, Ruiz A, Mukherjee P, Srikanth H, Phan MH (2013) Magneto-impedance biosensor with enhanced sensitivity for highly sensitive detection of nanomag-D beads. *IEEE Trans Magn* 49:4060–4063. doi:10.1109/TMAG.2012.2235414
- Devkota J, Ruiz A, Wingo J, Qin FX, Mukherjee P, Srikanth H, Phan MH (2014) Soft ferromagnetic microribbons with enhanced magnetoimpedance properties for high frequency sensor applications. *Phys Express* 4:10. <http://www.cognizure.com/pubs>
- Jang KJ, Kim CG, Yoon SS, Yu SC (2000) Effect of annealing field on asymmetric giant magnetoimpedance profile in Co-based amorphous ribbon. *J Magn Magn Mater* 215–216:488–491. doi:10.1016/S0304-8853(00)00200-6
- Kumar A, Mohapatra S, Miyar VF, Cerdeira A, Garcia JA, Srikanth H, Gass J, Kurlyandskaya GV (2007) Magnetoimpedance biosensor

- for Fe<sub>3</sub>O<sub>4</sub> nanoparticle intracellular uptake evaluation. *Appl Phys Lett* 91:143902. doi:[10.1063/1.2790370](https://doi.org/10.1063/1.2790370)
- Kurlyandskaya GV, Sanchez ML, Hernando B, Prida VM, Gorria P, Tejedor M (2003) Giant-magnetoimpedance-based sensitive element as a model for biosensors. *Appl Phys Lett* 82:3053–3055. doi:[10.1063/1.1571957](https://doi.org/10.1063/1.1571957)
- Li XP, Zhao ZJ, Chua C, Seet HL, Lu L (2003) Enhancement of giant magnetoimpedance effect of electroplated NiFe/Cu composite wires by dc Joule annealing. *J Appl Phys* 94:7626. doi:[10.1063/1.1628828](https://doi.org/10.1063/1.1628828)
- Makhnovskiy DP, Panina LV, Fry N, Mapps J (2004) Magnetoimpedance in NiFe/Au/NiFe sandwich films with different types of anisotropy. *J Magn Magn Mater* 272–276:1866. doi:[10.1016/j.jmmm.2003.12.833](https://doi.org/10.1016/j.jmmm.2003.12.833)
- Panina LV, Mohri K, Uchiyama T, Noda M (1995) Sensitive and quick response micro magnetic sensor utilizing magneto-impedance in Co-rich amorphous wires. *IEEE Trans Magn* 34:1249. doi:[10.1109/20.364817](https://doi.org/10.1109/20.364817)
- Phan MH, Peng HX (2008) Giant magnetoimpedance materials: fundamentals and applications. *Prog Mater Sci* 53:323. doi:[10.1016/j.pmatsci.2007.05.003](https://doi.org/10.1016/j.pmatsci.2007.05.003)
- Prida VM, Sánchez ML, Hernando B, Gorria P, Tejedor M, Vazquez M (2003) Influence of stress relief on hysteretic magnetoimpedance in Co-rich amorphous ribbons at the relaxation frequency. *Appl Phys A* 77:135–140. doi:[10.1007/s00339-002-2030-3](https://doi.org/10.1007/s00339-002-2030-3)
- Sommer RL, Chine CL (1996) Giant magneto-impedance effect in Metglas. *J Appl Phys* 79:5139. doi:[10.1063/1.361533](https://doi.org/10.1063/1.361533)
- Yang H, Chen L, Lei C, Zhang J, Li D, Zhou ZM, Bao CC, Hu HY, Chen X, Cui F, Zhang SX, Zhou Y, Cui DX (2010) *Appl Phys Lett* 97:043702. doi:[10.1063/1.3467833](https://doi.org/10.1063/1.3467833)
- Yang Z, Lei J, Lei C, Zhou Y, Wang T (2014) Effect of magnetic field annealing and size on the giant magnetoimpedance in micro-patterned co-based ribbon with a meander structure. *Appl Phys A* 116:1847–1851. doi:[10.1007/s00339-014-8343-1](https://doi.org/10.1007/s00339-014-8343-1)
- Zhou Y, Yu JQ, Zhao XL, Cai BC (2001) Giant magnetoimpedance in layered FeSiB/Cu/FeSiB films. *J Appl Phys* 89:1816–1819. doi:[10.1063/1.1338514](https://doi.org/10.1063/1.1338514)